

A Quantum Optimization Algorithm for Optimal Electric Vehicle Charging Station Placement for Intercity Trips

Tina Radvand

The University of Illinois at Urbana-Champaign
radvand2@illinois.edu

Alireza Talebpour

The University of Illinois at Urbana-Champaign
ataleb@illinois.edu

October 22, 2024

Abstract

Electric vehicles (EVs) play a significant role in enhancing the sustainability of transportation systems. However, their widespread adoption is hindered by inadequate public charging infrastructure, particularly to support long-distance travel. Identifying optimal charging station locations in large transportation networks presents a well-known NP-hard combinatorial optimization problem, as the search space grows exponentially with the number of potential charging station locations. This paper introduces a quantum search-based optimization algorithm designed to enhance the efficiency of solving this NP-hard problem for transportation networks. By leveraging quantum parallelism, amplitude amplification, and quantum phase estimation as a subroutine, the optimal solution is identified with a quadratic improvement in complexity compared to classical exact methods, such as branch and bound. The detailed design and complexity of a resource-efficient quantum circuit are discussed.

Keywords: Electric Vehicle, Charging Station Location, Grover’s Adaptive Search, Quantum Optimization

1 Introduction

According to the 2023 inventory of U.S. greenhouse gas (GHG) emissions and sinks [1], the transportation sector accounted for the highest proportion of total U.S. GHG emissions in 2021. Transportation is also a significant contributor to the presence of smog, soot, and air toxics in urban areas, which have profound health implications. Tightening of emission regulations [2] have urged the automotive industry to transition to more sustainable alternatives.

Electric vehicles (EVs) can be an effective solution to address the sustainability concerns associated with the transportation sector [3]. Having zero tailpipe emissions [4] and high energy conversion efficiency [5], operating with less noise level compared to internal combustion engines (ICE) [6], and promoting energy security by reducing dependence on imported energy sources [7] are some advantages of deploying EVs. Moreover, within the smart charging framework, EVs can potentially play a dual role by supporting the stability of the renewable energy grid [8] and providing power during grid stress through vehicle-to-grid capabilities [9].

While EVs offer numerous advantages, several concerns persist, impeding their broader adoption. As of 2022, electric vehicles accounted for less than 1% of cars in the United States [10]. The slow market penetration of electric vehicles can be attributed to several factors including their high purchase cost [11], long recharging time [12], short driving range (compared with ICE vehicles) [13], and lack or unreasonable distribution of charging facilities [14]. The last two factors, in particular, contribute to range anxiety among potential buyers [15]. The driving range offered by a fully charged battery of an electric vehicle is generally sufficient for the everyday needs of the majority of users. For example, in the U.S. approximately 95% of trips do not surpass 120 miles [16], whereas the average EV range is around 270 miles [17]. However, longer intercity trips cannot be completed on a single charge and necessitate the availability of public charging infrastructure

on interstate highways. Supporting such trips is also critical for long-haul freight as electric trucks are expected to become more widespread.

For long-distance trips, drivers regard the time spent waiting for charging as “deadtime” [18], emphasizing the importance of installing fast chargers to address these particular travels. Nevertheless, the installation and relocation of fast charging stations are costly [19]. Therefore, the optimal locations of charging infrastructure should be identified carefully, ensuring widespread access to EV owners.

Despite extensive research on the charging station location problem (CSLP) [20], it remains an NP-hard problem [21], and exact methods such as branch and bound fail to be effective in complex networks due to the vast number of feasible solutions in the search space [22]. For this reason, researchers often choose heuristic and metaheuristic approaches. While these methods provide feasible solutions, they often lead to suboptimal results due to their reliance on approximations and iterative processes that may not explore the entire solution space.

This study addresses these limitations by developing an exact quantum optimization algorithm to determine optimal charging station locations for long-distance trips. The optimization algorithm employs Grover Adaptive Search (GAS) [23] and Quantum Phase Estimation (QPE) [24] to find the optimal solution. It will be demonstrated that this technique has a computational complexity of $\mathcal{O}(1.4^n)$, where n is the number of candidate locations for charging stations. In contrast, classical algorithms offer computational complexity of $\mathcal{O}(2^n)$ for the same task. This paper is the first to design a gate-based quantum algorithm specifically for determining the optimal placement of charging stations in network settings. The algorithm is resource-efficient, utilizing a minimal number of ancillary quantum bits, which are restored and reused after each iteration.

The remainder of this paper is organized as follows: The **Literature Review** section examines classical techniques for CSLP and reviews quantum optimization techniques, particularly approaches that can be applied to solving CSLP. The **Problem Statement** section defines the problem, assumptions, and research objectives. The **Fundamentals of Quantum Computing** section provides a comprehensive overview of quantum computing principles and Grover Adaptive Search. The **Quantum Circuit Design** section details the development of a quantum algorithm

specifically for optimizing charging station placements in transportation networks. The **Analysis and Results** section applies the proposed algorithm to the central Illinois network, evaluating its accuracy and runtime. Finally, the **Conclusion and Future Path** section summarizes the key findings and suggests potential directions for future research.

2 Literature Review

The need for faster adoption of electric vehicles has led to an extensive body of literature on the charging station location problem. Unlike facility location problems, in which the demand is expressed as weights on nodes of a network, in most charging station location models, the demand is presented as a flow from an origin to a destination. The charging stations should be placed so that the distance between consecutive stations is within the driving range of electric vehicles.

Hodgson [25] was a pioneering figure in the study of location-allocation models by introducing the concept of flow-capturing demand. His model aimed to optimize the placement of facilities in order to maximize the coverage considering the demand. In this context, a particular demand is considered covered if there is at least one facility situated along the path from the origin to the destination. However, relying solely on a single charging facility between the origin and destination does not ensure that an electric vehicle will not face the risk of running out of charge.

Recognizing this limitation, Kuby and Lim [26] introduced the flow-refueling location model (FRLM). This model tackles the issue by generating a set of charging station combinations during a pre-processing step, ensuring that each trip to and from the destination becomes feasible. The primary objective of this model is to maximize the captured demand, taking into consideration that a trip is considered captured if at least one of the feasible combinations is utilized.

A key issue with implementing FRLM is the computational complexity associated with generating these combinations. Especially for large-scale networks, the process can be computationally intensive, requiring the application of heuristics to effectively address the problem [27]. To overcome this challenge, several other approaches have been proposed in the literature to solve the CSLP.

One such approach is the Arc covering model introduced by Capar [27], where a trip is considered

covered only if every arc along the route is covered by a charging station. Another approach was presented by MirHassani and Ebrazi [28], who expanded the network by constructing path segments from the origin to the destination and installing a charging station at the origin nodes. In order to guarantee trip feasibility, they ensured that the length of these path segments remained within the electric vehicle’s driving range.

Ghamami et al. [29] formulated a general corridor model as a mixed integer program with nonlinear constraints and solved it with a meta-heuristic algorithm based on simulated annealing. In their model, they tried to minimize the total system cost considering the queuing delay. Bao et al. [22] addressed a bi-level CSLP with a limited budget, ensuring that all vehicles completed their trips by selecting self-optimal routes while minimizing overall network congestion caused by potential detours. They employed both branch-and-bound and nested partitions algorithms, finding that branch-and-bound is well-suited for scenarios with short driving ranges. This finding is significant as it highlights how exact methods struggle to handle a large number of feasible solutions. In practice, these methods often resort to evaluating a large number of combinations, a challenge frequently encountered in realistic network scenarios.

Regardless of the modeling approach employed, CSLP is an NP-complete problem [21], and solving it in complex transportation networks poses significant challenges due to the numerous variables and constraints involved. Moreover, the objective function and constraints often exhibit non-linear behavior, making it difficult to find exact solutions within a reasonable time frame, which leads to the adoption of heuristic methods. Kchaou-Boujelben [20] has provided a comprehensive review and comparison of existing solution methods in their paper. In general, to reduce computational time, it is often necessary to make trade-offs in terms of solution quality. Given these challenges, recent advances in quantum computing offer a promising avenue worth exploring. This emerging technology may provide the computational power needed to overcome the computational complexity of the CSLP problem and deliver exact solutions rather than relying on heuristic methods.

Since the introduction of the first quantum computer model in 1980 [30], researchers have extensively explored the potential of quantum computing. Certain quantum algorithms, as shown in Table 1, have exhibited speed-ups over their classical counterparts. This quantum advantage

is not merely theoretical; recent breakthroughs demonstrate that scientists can efficiently solve problems using current noisy intermediate-scale quantum computers, achieving results beyond the reach of the most powerful supercomputers [31–35].

Table 1: Examples of Quantum Algorithms and Speed-Ups

Algorithm	Problem Definition	Speed-Up
Grover’s [36]	Searches an unsorted database containing N entries to locate a marked entry.	Quadratic
Simon’s [37]	Given $f : \{0, 1\}^n \rightarrow \{0, 1\}^n$, where $f(x) = f(y)$ if and only if $x \oplus y \in \{0^n, s\}$, finds $s \in \{0, 1\}^n$.	Exponential
Shor’s [38]	For an odd composite number, finds its integer factors.	Exponential
Quantum Phase Estimation [24]	Estimates the phase associated with an eigenvalue of a given unitary operator.	Exponential
Quantum Walk Search [39]	Finds a marked node in a graph G with N nodes, where a fraction ϵ are marked.	Quadratic
HHL [40]	Numerically solves a system of linear equations.	Exponential

Quantum optimization is among the fastest-growing areas in quantum computing research and multiple quantum optimization approaches exist. Quantum annealing (QA) [41] is a metaheuristic method for solving quadratic unconstrained binary optimization problems, making it suitable for problems with many local minima, such as the traveling salesman problem [42] and job-shop scheduling [43]. Quantum annealing machines, such as D-Wave Systems, map the optimization problem onto a quantum system, initialize it, and allow it to evolve adiabatically towards its optimal state. Quantum properties like tunneling help this technique overcome energy barriers and avoid getting trapped in local optima.

The Quantum Approximate Optimization Algorithm (QAOA) [44] is a heuristic approach that approximates solutions to combinatorial optimization problems, such as Max-Cut [44] and graph coloring [45]. While it has been widely explored in various applications, its performance bounds are still unknown.

Other techniques used in quantum optimization include the Variational Quantum Eigensolver (VQE) [46], which is particularly effective for quantum chemistry [47] and condensed matter physics problems [48]. Grover Adaptive Search (GAS) [23, 49] is another powerful method that excels in

tasks such as finding optimal solutions in large, unstructured spaces [50]. Additionally, Quantum Walks [51, 52] prove valuable in network analysis [53] and spatial search [54].

Despite decades of research into quantum optimization techniques and the development of various quantum algorithms, few researchers in the transportation field have applied these methods to accelerate the optimization of electric vehicle charging station placement.

Rao et al. [55] investigated the problem of charging station placement by incorporating both power grid and road network parameters, utilizing quantum annealing and the variational quantum eigensolver. Their results indicated that VQE did not achieve any notable speed-up. Although QA demonstrated runtime improvements—reportedly up to six times faster than classical methods—there are two significant challenges associated with this approach. First, tuning the penalty parameters is complex, as a large penalty can distort the solution landscape, while a small penalty may result in infeasible solutions [56]. Second, converting the constraint problem to an unconstrained form and generating the QUBO matrix is time-consuming and represents a bottleneck for the algorithm.

Chandra et al. [57] proposed a hybrid algorithm that combines quantum annealing with genetic algorithms. Similar to the previous case, calculating the penalty parameters for QA is computationally expensive.

In a recent work, Hu et al. [58] proposed an improved quantum genetic (IQGA) algorithm for placing charging stations to minimize the overall social cost. Their tests show that the IQGA approach has longer computation times due to the added overhead from simulated annealing, which may hinder its performance on large-scale problems.

Previous research on quantum computing approaches to the CSLP has predominantly focused on quantum annealing or heuristic algorithms. To date, no research has explored gate-based models such as Grover adaptive search for this problem. For an optimization problem with a search space of size N , Grover’s adaptive search has a worst-case time complexity of $O(\sqrt{N})$, offering a quadratic speedup compared to classical methods like branch and bound, which have a time complexity of $O(N)$ [59]. Moreover, unlike quantum annealing, Grover’s adaptive search does not face challenges related to choosing appropriate penalty terms and constructing a QUBO matrix.

The main challenge of Grover’s adaptive search lies in developing a quantum oracle capable of recognizing feasible solutions. This paper presents the step-by-step construction of a resource-efficient quantum circuit tailored for the CSLP problem in networks.

3 Problem Statement

This paper addresses the challenge of identifying optimal locations for fast charging stations to facilitate long-distance trips for electric vehicles within transportation networks. Specifically, given a set of origin–destination trips, \mathcal{Q} , the objective is to determine the combination of locations with the fewest charging stations. These stations must allow EVs with a driving range of R to complete each round-trip journey from origin to destination and back without running out of charge. The route for each trip is assumed to be predetermined, and the vehicle starts its journey with a half-full battery, following common practice in the literature.

The transportation network is modeled as graph $G = (\mathcal{N}, E)$ where \mathcal{N} is the set of nodes, representing possible locations for charging stations, and E is the set of edges, representing a direct connection between nodes. The length of each edge is the distance between nodes. For each path $q \in \mathcal{Q}$, \mathcal{N}_q is the set of nodes belonging to trip q . In addition to the network nodes, two auxiliary nodes are introduced: O , which is connected to all trip origins, and D , which is connected to all trip destinations. The edges connecting the auxiliary nodes to the network have a length of 0.

For a given node $i \in \mathcal{N}_q \cup \{O, D\}$, the accessible set A_i^q comprises nodes that appear after i on the path q and are within a distance less than the predetermined threshold value R from node i . The first condition ensures that the vehicle does not move backward in its path. The second condition identifies the nodes that are accessible from node i , assuming the vehicle departs from node i with a full battery. As there are no nodes after the destination, the accessible set for the destination is always empty, i.e., $A_D^q = \emptyset \quad \forall q \in \mathcal{Q}$. Additionally, considering that the vehicle starts its trip with a half-full battery, the accessible nodes for node O must be within a distance of $R/2$. In this problem, there is no need to explicitly check for the return trip. As long as the electric vehicle has at least half of its battery capacity remaining when reaching the destination, it

can refuel at the same charging station while traveling in the opposite direction back to the origin. To ensure a successful return trip, any node that includes node D in its accessible set should be within a distance of $R/2$. This problem is formulated as follows:

$$\text{Minimize } \sum_{i \in \mathcal{N}} S_i \tag{1}$$

$$\text{subject to } (1 - S_i) + \sum_{j \in A_i^q} S_j \geq 1 \quad \forall q \in \mathcal{Q}, \forall i \in \mathcal{N}_q \cup \{O\} \tag{2}$$

$$S_O = 1 \tag{3}$$

$$S_D = 1 \tag{4}$$

$$S_i \in \{0, 1\} \quad \forall i \in \mathcal{N} \tag{5}$$

The objective function (1) minimizes the total number of charging stations selected. Constraint (2) ensures that the vehicle will visit a charging station or the destination before running out of charge. Constraints (3) and (4) requires that each trip starts from the origin and ends at the destination. Finally, constraint (5) states that each decision variable S_i is binary. Table 2 summarizes the parameters used.

Table 2: Model Parameters

Parameter	Description
\mathcal{Q}	Set of origin–destination trips taken by EV drivers in the network
q	A specific trip, where $q \in \mathcal{Q}$.
R	Range of electric vehicles
A_i^q	Set of accessible nodes for node i on path q
\mathcal{N}	Set of nodes of network G
E	Set of edges of network G
\mathcal{N}_q	Set of nodes belonging to trip q
O	Auxiliary node connected to all trip origins
D	Auxiliary node connected to all trip destinations
Decision Variables	
S_i	Binary station location variable; $S_i = 1$ if station is located at node i , $S_i = 0$ otherwise

4 Fundamentals of Quantum Computing

This section begins with an introduction to the key concepts in quantum computing relevant to this study, including qubits and superpositions, followed by an explanation of how to perform computations using quantum gates. Grover's search algorithm, which serves as a building block for Grover's adaptive search optimization, is then introduced. This section concludes with a description of the GAS algorithm.

4.1 Qubit and Superposition

A quantum bit, or qubit, is the quantum mechanical analogue of a classical bit and is the fundamental unit of quantum computers. Two possible states for a qubit are $|0\rangle = \begin{bmatrix} 1 \\ 0 \end{bmatrix}$ and $|1\rangle = \begin{bmatrix} 0 \\ 1 \end{bmatrix}$, which are known as computational basis states. In this notation, $|\ \rangle$ is called a *ket*, representing a quantum state as a column vector, while $\langle \ |$ is known as a *bra*, denoting the corresponding row vector. One interesting difference between bits and qubits is that while bits can only be in states 0 or 1, qubits can exist in any linear combination of these states, known as superpositions:

$$|\psi_1\rangle = \alpha_0 |0\rangle + \alpha_1 |1\rangle = \begin{bmatrix} \alpha_0 \\ \alpha_1 \end{bmatrix} \quad (6)$$

Where α_0 and α_1 are complex numbers, representing the amplitudes of states $|0\rangle$ and $|1\rangle$, respectively. When a measurement is performed on this qubit, the superposition collapses, and the result of the measurement will be either the state $|0\rangle$ with probability $|\alpha_0|^2$ or $|1\rangle$ with probability $|\alpha_1|^2$. Notably, the probabilities $|\alpha_0|^2$ and $|\alpha_1|^2$ satisfy the normalization condition, i.e., $|\alpha_0|^2 + |\alpha_1|^2 = 1$. The concept of superposition can be expanded for a k -level system, denoted by

$|0\rangle, |1\rangle, |2\rangle, \dots, |k-1\rangle$. An arbitrary qubit in this system can be expressed as:

$$|\psi_2\rangle = \alpha_0 |0\rangle + \alpha_1 |1\rangle + \dots + \alpha_{k-1} |k-1\rangle = \begin{bmatrix} \alpha_0 \\ \alpha_1 \\ \vdots \\ \alpha_{k-1} \end{bmatrix} \quad (7)$$

Where $\sum_{i=1}^{k-1} |\alpha_i|^2 = 1$. Transitioning from the single-qubit system to n qubits, the general quantum state can be written as:

$$|\psi_3\rangle = \sum_{x \in \{0,1\}^n} \alpha_x |x\rangle \quad (8)$$

Where, $\sum_{x \in \{0,1\}^n} |\alpha_x|^2 = 1$. For instance, when $n = 2$, the quantum state can be expressed as:

$$\alpha_{00} |00\rangle + \alpha_{01} |01\rangle + \alpha_{10} |10\rangle + \alpha_{11} |11\rangle \quad (9)$$

Superposition is crucial for making quantum computers powerful. It allows quantum systems to simultaneously exist in multiple states, in contrast to classical systems that are limited to a single state. This property enables quantum parallelism, where applying a function to the system's state affects all states at once.

4.2 Unitary Operations and Quantum Gates

To perform calculations, qubits—represented as vectors in a two-dimensional complex vector space—are manipulated through operations performed by matrices. To ensure conservation of probabilities, these operators, known as gates, must be unitary. The operators used in this paper are introduced below.

4.2.1 Pauli-X Gate

One quantum gate is the Pauli-X gate, also known as the quantum NOT gate. It acts as a qubit flipper, transforming $|0\rangle$ to $|1\rangle$ and $|1\rangle$ to $|0\rangle$. The effect of a Pauli-X gate on the state $|\psi_1\rangle =$

$\alpha_0 |0\rangle + \alpha_1 |1\rangle$ is shown below:

$$X|\psi_1\rangle = \begin{bmatrix} 0 & 1 \\ 1 & 0 \end{bmatrix} \begin{bmatrix} \alpha_0 \\ \alpha_1 \end{bmatrix} = \begin{bmatrix} \alpha_1 \\ \alpha_0 \end{bmatrix} = \alpha_1 |0\rangle + \alpha_0 |1\rangle \quad (10)$$

$$\alpha_0 |0\rangle + \alpha_1 |1\rangle \text{ --- } \boxed{X} \text{ --- } \alpha_1 |0\rangle + \alpha_0 |1\rangle$$

Figure 1: Representation of a Pauli-X gate. The X gate flips the state of a qubit from $|0\rangle$ to $|1\rangle$ and vice versa.

Figure 1 shows a representation of the Pauli-X gate in a quantum circuit.

4.2.2 Hadamard Gate

The Hadamard gate is a fundamental quantum gate that plays a crucial role in creating quantum superposition states. The matrix representation of this gate is:

$$H = \frac{1}{\sqrt{2}} \begin{bmatrix} 1 & 1 \\ 1 & -1 \end{bmatrix} \quad (11)$$

When applied to the $|0\rangle$ state, the Hadamard gate maps it to the superposition state $|+\rangle = \frac{|0\rangle+|1\rangle}{\sqrt{2}}$:

$$H|0\rangle = \frac{1}{\sqrt{2}} \begin{bmatrix} 1 & 1 \\ 1 & -1 \end{bmatrix} \begin{bmatrix} 1 \\ 0 \end{bmatrix} = \frac{1}{\sqrt{2}} \begin{bmatrix} 1 \\ 1 \end{bmatrix} = \frac{1}{\sqrt{2}}(|0\rangle + |1\rangle) = |+\rangle. \quad (12)$$

Similarly, when applied to the $|1\rangle$ state, it maps it to the superposition state $|-\rangle = \frac{|0\rangle-|1\rangle}{\sqrt{2}}$:

$$H|1\rangle = \frac{1}{\sqrt{2}} \begin{bmatrix} 1 & 1 \\ 1 & -1 \end{bmatrix} \begin{bmatrix} 0 \\ 1 \end{bmatrix} = \frac{1}{\sqrt{2}} \begin{bmatrix} 1 \\ -1 \end{bmatrix} = \frac{1}{\sqrt{2}}(|0\rangle - |1\rangle) = |-\rangle. \quad (13)$$

In other words, the Hadamard gate puts a qubit into an equal superposition of the $|0\rangle$ and $|1\rangle$ states. Figure 2 shows a representation of the Hadamard gate in a quantum circuit.

$$\alpha_0 |0\rangle + \alpha_1 |1\rangle \longrightarrow \boxed{H} \longrightarrow \alpha_0 |+\rangle + \alpha_1 |-\rangle$$

Figure 2: Representation of a Hadamard gate. The Hadamard gate creates a superposition state by transforming $|0\rangle$ to $|+\rangle$ and $|1\rangle$ to $|-\rangle$.

4.2.3 CNOT Gate

The CNOT gate is a two-qubit gate where the first qubit is the control qubit and the second qubit is the target qubit. The gate flips the state of the target qubit if the control qubit is in the state $|1\rangle$; otherwise, the target qubit remains unchanged. The effect of the CNOT gate on the state $|\psi_1\rangle = \alpha_0 |0\rangle + \alpha_1 |1\rangle$, with control qubits $|0\rangle$ and $|1\rangle$, is shown below:

$$\text{CNOT}(\alpha_0 |00\rangle + \alpha_1 |01\rangle) = \begin{bmatrix} 1 & 0 & 0 & 0 \\ 0 & 1 & 0 & 0 \\ 0 & 0 & 0 & 1 \\ 0 & 0 & 1 & 0 \end{bmatrix} \begin{bmatrix} \alpha_0 \\ \alpha_1 \\ 0 \\ 0 \end{bmatrix} = \begin{bmatrix} \alpha_0 \\ \alpha_1 \\ 0 \\ 0 \end{bmatrix} = \alpha_0 |00\rangle + \alpha_1 |01\rangle \quad (14)$$

$$\text{CNOT}(\alpha_0 |10\rangle + \alpha_1 |11\rangle) = \begin{bmatrix} 1 & 0 & 0 & 0 \\ 0 & 1 & 0 & 0 \\ 0 & 0 & 0 & 1 \\ 0 & 0 & 1 & 0 \end{bmatrix} \begin{bmatrix} 0 \\ 0 \\ \alpha_0 \\ \alpha_1 \end{bmatrix} = \begin{bmatrix} 0 \\ 0 \\ \alpha_1 \\ \alpha_0 \end{bmatrix} = \beta |10\rangle + \alpha |11\rangle \quad (15)$$

Figure 3 shows a representation of the CNOT gate in a quantum circuit.



Figure 3: Representation of CNOT gate. (A) When the control qubit is $|0\rangle$, the target qubit remains unchanged. (B) When the control qubit is $|1\rangle$, the target qubit is flipped.

4.2.4 Phase Gate

Phase gate maps $|0\rangle$ to itself, and $|1\rangle$ to $e^{\frac{2\pi i}{2^n}}|1\rangle$. The probability of measuring either $|0\rangle$ or $|1\rangle$ remains unchanged by the application of this gate.

$$R_n = \begin{bmatrix} 1 & 0 \\ 0 & e^{\frac{2\pi i}{2^n}} \end{bmatrix}. \quad (16)$$

It is evident that $|0\rangle$ and $|1\rangle$ are eigenvectors of R_n . Figure 4 shows a representation of a phase gate in a quantum circuit.

$$\alpha|0\rangle + \beta|1\rangle \text{ --- } \boxed{R_n} \text{ --- } \alpha|0\rangle + e^{\frac{2\pi i}{2^n}}\beta|1\rangle$$

Figure 4: Representation of the phase gate: $|0\rangle$ remains unchanged, while $|1\rangle$ is mapped to $e^{\frac{2\pi i}{2^n}}|1\rangle$.

4.3 Grover's Search Algorithm

Consider an unstructured dataset containing $N = 2^n$ elements, denoted as S_0, S_1, \dots, S_{N-1} . Within this dataset, M elements, where $1 \leq M \leq N$, satisfy a Boolean condition denoted as f . The objective is to identify an element S_v for which $f(S_v) = 1$. Grover's search algorithm [36] provides a method for solving this problem, reducing the complexity from $\mathcal{O}(N)$ operations in classical algorithms to $\mathcal{O}(\sqrt{N})$ operations.

This dataset can be stored in a quantum system, where the amplitudes of each state correspond to the probability of observing that state. Given that the probability of randomly picking any state is $\frac{1}{N}$, the initial state of the system, $|\psi\rangle$, is given by:

$$|\psi\rangle = \frac{1}{\sqrt{N}} \sum_{i=0}^{N-1} |S_i\rangle \quad (17)$$

Figure 5a illustrates that the amplitudes of all states are equal, thus the probability of measuring each state is the same. We define normalized states $|\bar{\omega}\rangle$ and $|\omega\rangle$ to span the initial state, $|\psi\rangle$, to the

non-solution and solution states, respectively.

$$|\psi\rangle = \frac{1}{\sqrt{N}} \left(\sum_{\substack{i=0 \\ f(S_i)=0}}^{N-1} |S_i\rangle + \sum_{\substack{i=0 \\ f(S_i)=1}}^{N-1} |S_i\rangle \right) = \sqrt{\frac{N-M}{N}} |\bar{\omega}\rangle + \sqrt{\frac{M}{N}} |\omega\rangle \quad (18)$$

Where $|\bar{\omega}\rangle$ and $|\omega\rangle$ are:

$$|\bar{\omega}\rangle = \frac{1}{\sqrt{N-M}} \sum_{\substack{S_i \\ f(S_i)=0}} |S_i\rangle \quad (19)$$

$$|\omega\rangle = \frac{1}{\sqrt{M}} \sum_{\substack{S_i \\ f(S_i)=1}} |S_i\rangle \quad (20)$$

Figure 5b illustrates this spanning, where $\frac{\theta}{2}$ represents the angle between the initial state and $|\bar{\omega}\rangle$, and $\sin \frac{\theta}{2} = \sqrt{\frac{M}{N}}$. When $M \ll N$, $\sin \frac{\theta}{2} \approx \frac{\theta}{2} = \sqrt{\frac{M}{N}}$.

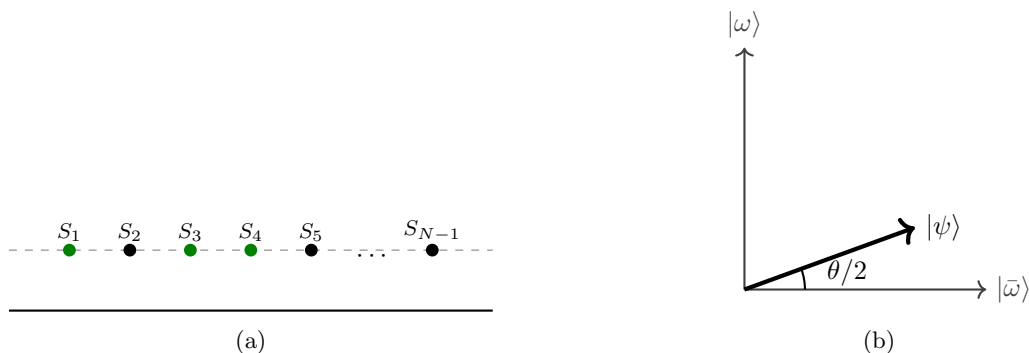


Figure 5: Illustration of the initial superposition state in Grover's algorithm. (A) Solution states (green dots) and non-solution states (black dots) illustrating uniform amplitudes. The dashed line represents the mean amplitude of the system. (B) Representation of the state vector $|\psi\rangle$ spanning across solution $|\omega\rangle$ and non-solution spaces $|\bar{\omega}\rangle$.

The amplitudes of $|\bar{\omega}\rangle$ and $|\omega\rangle$ in Eq. (18) indicate that the probability of measuring a non-solution state is $\frac{N-M}{N}$, while the probability of measuring a solution state is $\frac{M}{N}$. The ingenuity of Grover's algorithm lies in its ability to transform this initial state in a way that increases the probability of measuring the solution states.

In order to enhance the probability of measuring $|\omega\rangle$, it is necessary to first identify it. This step is accomplished through the introduction of a quantum oracle (O). For now, we treat the oracle as

a black box whose action is to mark the solution states, by utilizing a phase qubit $|\varphi\rangle$:

$$|S_i\rangle |\varphi\rangle \xrightarrow{O} |S_i\rangle |\varphi \oplus f(S_i)\rangle \quad (21)$$

where \oplus denotes exclusive OR (XOR) or addition modulo 2. When the state $|\varphi\rangle$ is initialized to $|-\rangle$,

$$|-\oplus f(S_i)\rangle = \frac{|0\oplus f(S_i)\rangle - |1\oplus f(S_i)\rangle}{\sqrt{2}} = \begin{cases} |-\rangle & \text{if } f(S_i) = 0 \\ -|-\rangle & \text{if } f(S_i) = 1 \end{cases} \quad (22)$$

Substituting Equation (22) into Equation (21) yields:

$$|S_i\rangle |-\rangle \xrightarrow{O} (-1)^{f(S_i)} |S_i\rangle |-\rangle \quad (23)$$

This initialization causes the oracle to effectively mark the solution states by altering their phase while keeping the phase qubit unaffected. The action of the oracle gate can be summarized as:

$$O \left(\sqrt{\frac{N-M}{N}} |\bar{\omega}\rangle + \sqrt{\frac{M}{N}} |\omega\rangle \right) = \sqrt{\frac{N-M}{N}} |\bar{\omega}\rangle - \sqrt{\frac{M}{N}} |\omega\rangle \quad (24)$$

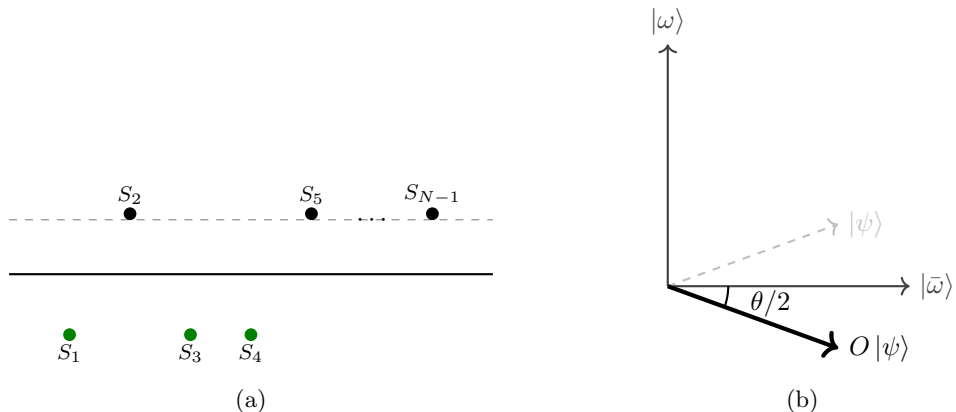


Figure 6: Illustration of the quantum state after applying the oracle operator in Grover's algorithm. (A) Solution states' amplitudes are inverted, while non-solution states retain their original amplitudes. The dashed line represents the mean amplitude of the system. (B) Quantum state is reflected around the $|\bar{\omega}\rangle$ axis after the oracle operation.

The effect of the oracle on the state of the system is illustrated in Figure 6. After applying the oracle, the next step in Grover's algorithm involves transforming the qubits using the diffuser operator, $2|+^n\rangle\langle +^n| - I$. This operator reflects any arbitrary quantum state, previously introduced as $|\psi_3\rangle = \sum_{x \in \{0,1\}^n} \alpha_x |x\rangle$, about its mean amplitude $\mu = \frac{1}{N} \sum_{x \in \{0,1\}^n} \alpha_x$, where $N = 2^n$. The operator's impact on the quantum state is shown through the following derivation:

$$\begin{aligned} (2|+^n\rangle\langle +^n| - I)|\psi_3\rangle &= \frac{2}{\sqrt{N}} \sum_{x \in \{0,1\}^n} |x\rangle \left(\frac{1}{\sqrt{N}} \sum_{x \in \{0,1\}^n} \langle x| \sum_{x \in \{0,1\}^n} \alpha_x |x\rangle \right) - \sum_{x \in \{0,1\}^n} \alpha_x |x\rangle = \\ \frac{2}{N} \sum_{x \in \{0,1\}^n} |x\rangle \left(\sum_{x \in \{0,1\}^n} \alpha_x \right) - \sum_{x \in \{0,1\}^n} \alpha_x |x\rangle &= \sum_{x \in \{0,1\}^n} (2\mu - \alpha_x) |x\rangle \end{aligned} \quad (25)$$

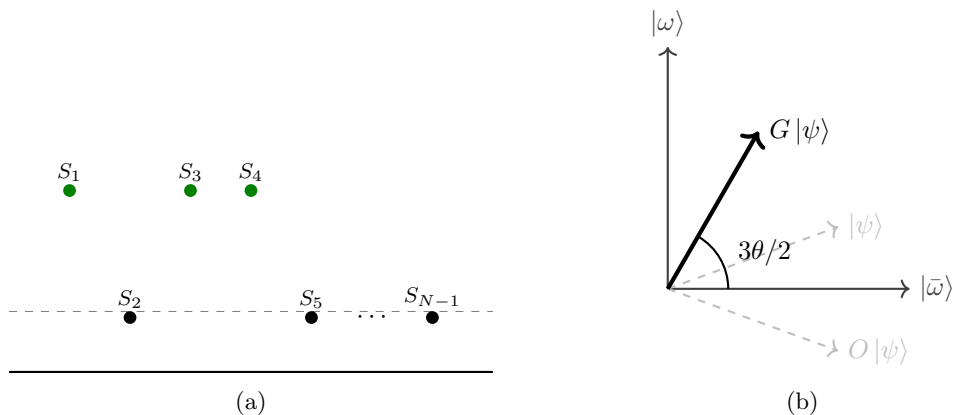


Figure 7: Illustration of the quantum state after applying the diffuser operator in Grover's algorithm. (A) All states are reflected about the mean amplitude. The dashed line represents the mean amplitude of the system. (B) Quantum states are reflected about the mean amplitude.

In the literature, it is customary to represent the combination of oracle and the diffuser as the Grover iteration G , where $G(|\psi\rangle) = (2|+^n\rangle\langle +^n| - I)O(|\psi\rangle)$. As evident in Figure 7, a single application of the Grover iteration rotates the state towards the answer. If we apply the operator G for k times, the resulting state can be expressed as:

$$G^k |\psi\rangle = \left(\cos \frac{2k+1}{2} \theta \right) |\bar{\omega}\rangle + \left(\sin \frac{2k+1}{2} \theta \right) |\omega\rangle \quad (26)$$

This algorithm approaches the desired solution when $\sin \frac{2k+1}{2} \theta$ is close to 1, or when $\frac{2k+1}{2} \theta \approx \frac{\pi}{2}$.

Thus, If K denotes the number of iterations required to maximize the amplitude of the solution state, the following inequality holds:

$$K \leq \left\lceil \frac{\pi}{4} \sqrt{\frac{N}{M}} \right\rceil \quad (27)$$

This result demonstrates that a quantum search algorithm requires $\mathcal{O}\left(\sqrt{\frac{N}{M}}\right)$ oracle calls, showcasing a quadratic improvement over the $\mathcal{O}\left(\frac{N}{M}\right)$ requirement for classical computers.

In Grover’s algorithm, it is assumed that the number of solution states, M , is known. However, that is often not the case in practice. Shortly after Grover introduced his search algorithm, Boyer et al.,[59] developed an algorithm to find the solutions even when the number of solutions (M) is unknown. Algorithm 1 illustrates this approach, which is often referred to as quantum exponential search in the literature.

Algorithm 1 Quantum Exponential Search [59]

```

1: Initialize  $m \leftarrow 1$  and  $\lambda \leftarrow \frac{8}{7}$  ▷ Any value of  $\lambda$  strictly between 1 and  $\frac{4}{3}$  would work.
2: while True do
3:   Choose  $j \in \{0, 1, \dots, m - 1\}$  uniformly at random
4:   Apply  $j$  iterations of Grover’s algorithm
5:   Observe the register and let  $S_i$  be the outcome
6:   if  $f(S_i) = 1$  then
7:     return  $S_i$ 
8:   else
9:      $m \leftarrow \min(\lambda m, N)$ 
10:  end if
11: end while

```

4.4 Grover’s Adaptive Search

Grover’s Adaptive Search [23] is an algorithm that employs quantum exponential search as a subroutine to find the optimal solution in an optimization problem. There is an unstructured dataset with elements S_0, S_1, \dots, S_{N-1} and a function f such that $f(S_\nu) = 1$ indicates S_ν is a valid solution. Additionally, there is a function T that assigns a cost to each state. The goal of Grover’s Adaptive Search is to find the state S_ν such that $f(S_\nu) = 1$ and $T(S_\nu)$ is minimized. Algorithm 2 presents the steps of Grover’s Adaptive Search. This algorithm searches for solutions with costs below a threshold. This threshold is updated at every step of the algorithm. The algorithm returns the true

minimum value with a probability of $1/2$, but this probability can be increased by repeating the algorithm a constant number of times. In each iteration, the threshold τ is randomly selected from the range 0 to the result of the previous iteration. This process solves the problem using $O(\sqrt{N})$ probes.

Algorithm 2 Grover’s Adaptive Search [23]

- 1: Choose a threshold index $0 \leq \tau \leq N - 1$ uniformly at random
 - 2: **while** total running time $\leq 22.5\sqrt{N} + 1.4 \log^2 N$ **do**
 - 3: Initialize the states
 - 4: Run exponential search with an oracle that marks states S_j where $T(S_j) < T(S_\tau)$
 - 5: Save the return value of the search in $S_{\tau'}$
 - 6: **if** $T(S_{\tau'}) < T(S_\tau)$ **then**
 - 7: Set the threshold index $\tau \leftarrow \tau'$
 - 8: **end if**
 - 9: **end while**
 - 10: **return** S_τ
-

5 Quantum Circuit Design

In Grover’s search algorithm (4.3) and Grover’s adaptive search (4.4), the Boolean function f and the cost function T are treated as black boxes. To apply these algorithms effectively, these functions must be tailored to the specific problem being addressed. An optimal design should aim to be resource-efficient, minimizing the number of qubits and gates required.

This section presents the quantum circuit design for identifying valid combinations (combinations that can support the trips, i.e., function f) and counting the number of charging stations in each combination (function T). These circuits are then used to find the optimal combination using GAS.

5.1 Identifying Valid Combinations

This section provides a detailed explanation of the quantum circuit design for identifying and marking valid combinations. The process is initially described for single corridors, followed by an extension to networks with multiple origins and destinations.

Figure 8 illustrates a route from node 1 to node 4, where potential charging station locations are nodes 1, 2, 3, and 4. The electric vehicle considered in this scenario has a driving range of 100 km. The objective is to design a quantum circuit that identifies the valid placements of charging stations along this path. The logic employed for this example can be extended to charging station placements along any given path.

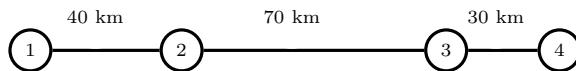


Figure 8: Route from 1 to 4 with potential charging stations at nodes 1, 2, 3, and 4.

The presence or absence of a charging station at each node is represented by a qubit denoted as S_i , where i corresponds to the node label:

$$|S_i\rangle = \begin{cases} |1\rangle & \text{if there is a charging station at node } i \\ |0\rangle & \text{if there is no charging station at node } i \end{cases} \quad (28)$$

In addition to these qubits, two additional qubits, S_O and S_D , represent the origin and destination nodes, respectively. Figure 9 illustrates the expanded version of the route, encompassing the origin and destination nodes, indicated by dashed circles. When these qubits are $|1\rangle$, it signifies that the vehicle has reached these nodes. Since O and D serve as auxiliary nodes for 1 and 2, respectively, their distance to these nodes is defined as 0. The definition of accessible sets was introduced in Section 3. Table 3 presents the accessible sets for each node in the example graph.

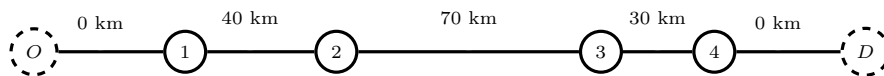


Figure 9: Expanded route with the origin(O) and destination(D) nodes shown as dashed circles.

This example consists of 2^4 different combinations for placing charging stations, some of which can be valid. Each combination is represented as a quantum state in the form of $|S_D S_4 S_3 S_2 S_1 S_O\rangle$. $|S_D S_4 S_3 S_2 S_1 S_O\rangle$ is considered a valid solution if it starts at the origin and ends at the destination, i.e., $|S_O\rangle = |S_D\rangle = |1\rangle$, and does not contain an isolated charging station. Specifically, if $|S_i\rangle = |1\rangle$,

Table 3: Accessible sets for nodes in the example corridor.

Node	Accessible Set
O	$\{1, 2\}$
1	$\{2\}$
2	$\{3, 4\}$
3	$\{4, D\}$
4	$\{D\}$
D	\emptyset

then at least one element in the accessible set of node i must also be in the state $|1\rangle$.

In the following, the design details of a quantum circuit that can mark valid combinations are described. The circuit involves (1) initializing qubits, (2) utilizing ancilla qubits to identify combinations containing isolated nodes, (3) distinguishing valid states, and finally (4) reversing operations and resetting ancilla qubits to $|0\rangle$.

5.1.1 Initialization:

IBM’s Qiskit software was utilized to build and simulate quantum circuits due to its comprehensive and user-friendly framework. In Qiskit, the default state of a qubit is $|0\rangle$. To ensure that all the different combinations of charging station locations are constructed with equal probability, the Hadamard gate is applied to the qubits representing the possible locations of charging stations. In addition, to ensure that the vehicle starts its trip from the origin and reaches the destination, $|S_O\rangle$ and $|S_D\rangle$ are set to $|1\rangle$ using the quantum Not gate. Ancillary qubits, $|anc\rangle$, and the validity qubit, $|v_1\rangle$, remain in their initial state. The result of applying these gates to the initial state $|0\rangle^{\otimes 12}$ is:

$$X \otimes H^{\otimes 4} \otimes X \otimes I^{\otimes 6} |0\rangle^{\otimes 12} = \frac{1}{\sqrt{2^4}} \sum_{x \in \{0,1\}^4} |1\rangle |x\rangle |1\rangle |0\rangle^{\otimes 6} \quad (29)$$

Here, the tensor product symbol (\otimes) between the operators indicates that these operations are applied independently to each qubit. Figure 10 illustrates the initialization component of the oracle.

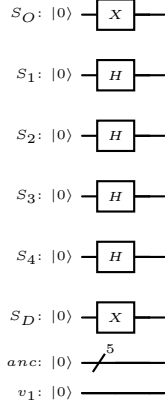


Figure 10: Qubits Initialization: $|S_O\rangle$ and $|S_D\rangle$ are initialized to $|1\rangle$. $|S_i\rangle$ for $i \in \{1, 2, 3, 4\}$ are initialized to $|+\rangle$. Ancillary qubits and the validity qubit $|v_1\rangle$ are in state $|0\rangle$.

5.1.2 Isolated Charging Station Detection

An isolated charging station is defined as a charging station where a vehicle charges but will exhaust its charge before reaching the next charging station. This condition arises when a node is in state $|1\rangle$ while all other nodes in its accessible set are in state $|0\rangle$.

After initializing the qubits, the circuit evaluates each node to detect isolated nodes and records this information in ancillary qubits. For a corridor with a total of n candidate places for charging stations, $n + 1$ ancillary qubits are required: one for each node and an additional one for the origin node O . The destination node is excluded from checking as its accessible set is always empty.

Figure 11 illustrates part of the oracle circuit that checks whether each node is isolated or not. For node O , nodes 1 and 2 fall within its accessible range. A multi-qubit controlled-NOT gate flips the first ancillary qubit anc_1 when node O is in state $|1\rangle$ and its accessible nodes are in state $|0\rangle$. Thus, an ancillary qubit in state $|1\rangle$ indicates that the corresponding node is isolated. After applying the X gate to flip the accessible nodes, these nodes are restored to their original states by applying the X gate once more.

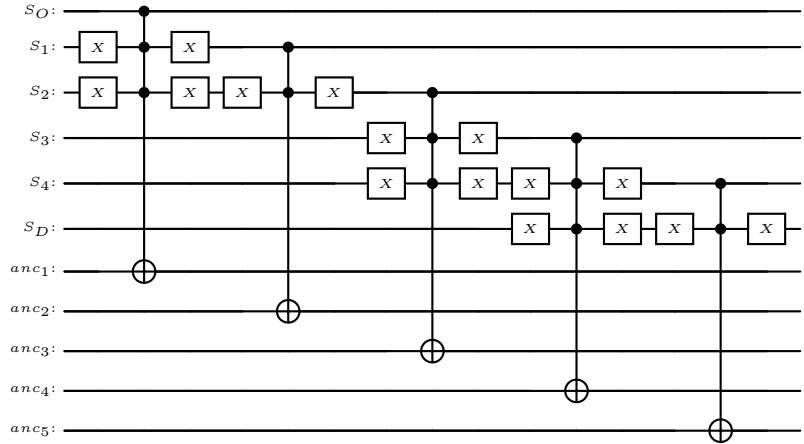


Figure 11: Isolated Charging Station Detection: When a node is isolated, its corresponding ancillary qubit switches to $|1\rangle$.

5.1.3 Labeling Valid Combinations:

A combination is considered valid if it contains no isolated charging stations, or if all the ancillary qubits are in state $|0\rangle$. Figure 12 illustrates the labeling process. The ancillary qubits are inspected to ensure that any flipped ancillary qubits are in state $|1\rangle$. If this condition is satisfied, the combination is validated, and the validity qubit is flipped using a multi-qubit controlled-NOT gate. Subsequently, the ancillary qubits are returned to their original state by applying the X gate.

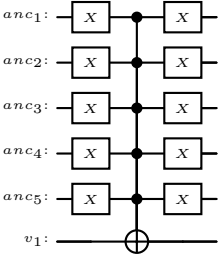


Figure 12: Labeling Valid Combinations: The validity qubit $|v_1\rangle$ is flipped when all ancillary qubits are in state $|0\rangle$.

5.1.4 Restoration of Ancillary Qubits

Restoration of ancillary qubits involves bringing them back to state $|0\rangle$. This enables the reuse of these qubits in subsequent steps of the algorithm, thereby reducing the total number of qubits required. Restoration is achieved by reversing the operations in the isolation detection and labeling step, i.e., applying the gates in Figure 11 and Figure 12 in reverse order. Figure 13 shows the circuit used for this restoration.

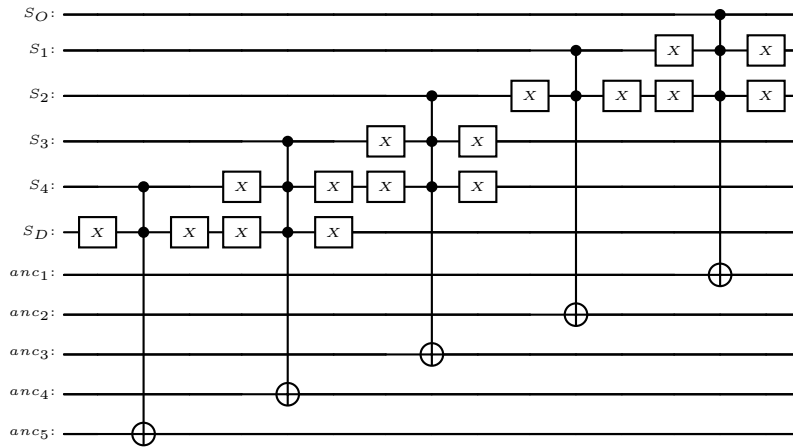


Figure 13: Restoration of Ancillary Qubits

Integrating the previously described steps results in a quantum circuit capable of marking all valid combinations. Figure 14 illustrates the quantum circuit for finding valid charging station placements for a single path.

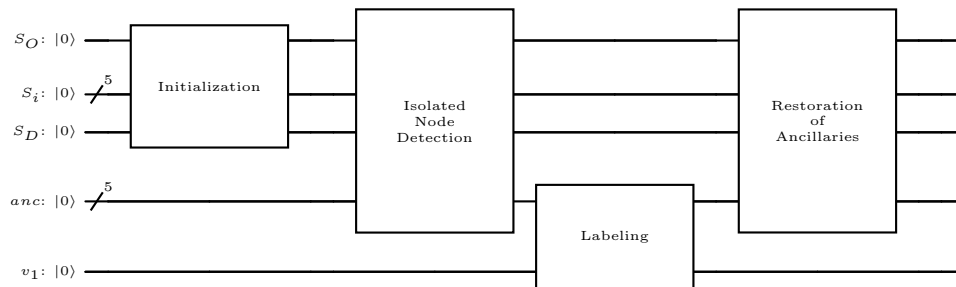


Figure 14: Quantum circuit for identifying valid charging station placements on a single path.

Extending the approach from a single path to a network with multiple paths is straightforward. For a network with $|\mathcal{Q}|$ paths, all paths must be valid, i.e., all validity qubits should be in the state $|1\rangle$. Figure 15 illustrates the corresponding quantum circuit for a network with m nodes and $|\mathcal{Q}|$ O-D pairs. In this circuit, the validity qubit of each trip is flipped when the combination can support the trip. Ultimately, the qubit v_T is flipped if all paths are traversable. The qubit restoration process is performed by applying all the gates in reverse order. The total number of qubits required is $(|\mathcal{Q}| + 1)(n + 2) + 1$.

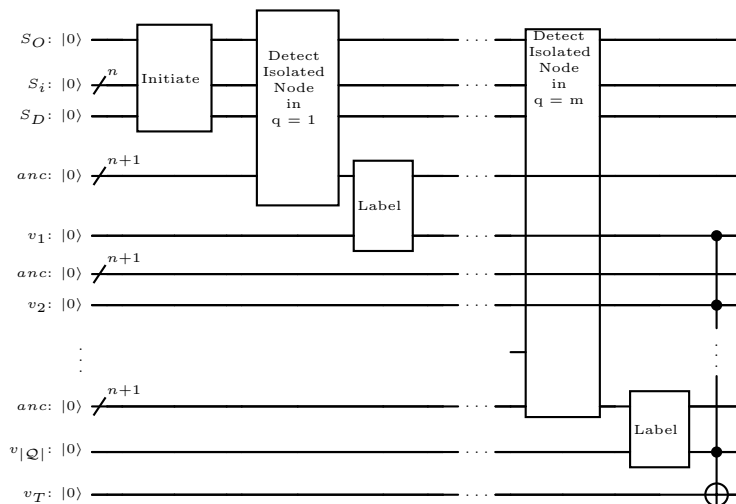


Figure 15: Quantum circuit for identifying valid charging station placements on a network with n possible locations and $|\mathcal{Q}|$ O-D trips.

5.2 Station Counting

This section extends the previously developed quantum oracle to count the number of charging stations in each combination, followed by the application of a quantum minimization algorithm to identify the combination with the fewest charging stations.

5.2.1 Counting Charging Stations

Given a combination $|S_n \dots S_2 S_1\rangle$, the objective is to determine the number of ones it contains. This quantity is known as the Hamming weight of the state and is denoted by \mathcal{H} . This can be achieved with the help of Quantum Phase Estimation (QPE). QPE is an efficient algorithm to estimate the eigenvalues of a unitary operator. Unitary operators are operators whose eigenvalues have modulus one. Thus, if $|\nu\rangle$ is an eigenvector for a unitary operator U , we can write $U|\nu\rangle = e^{2\pi i\theta}|\nu\rangle$. Here, θ represents the phase of U . For $U = R_n^{\otimes n}$,

$$R_n^{\otimes n} |S_n \dots S_2 S_1\rangle = \left(\prod_{j=1}^n e^{\frac{2\pi i S_j}{2^n}} \right) |S_n \dots S_2 S_1\rangle = e^{\frac{2\pi i \sum_n S_j}{2^n}} |S_n \dots S_2 S_1\rangle \quad (30)$$

By estimating the phase of $R_n^{\otimes n}$ using QPE, the number of ones in the state, $\sum_n S_j$, can be determined. Figure 16 illustrates the implementation of QPE using the operator $R_n^{\otimes n}$. The algorithm necessitates n ancillary qubits. However, by the conclusion of the computation, at most $\lceil \log(n+1) \rceil$ of these qubits are altered, while the remaining qubits stay in state 0.

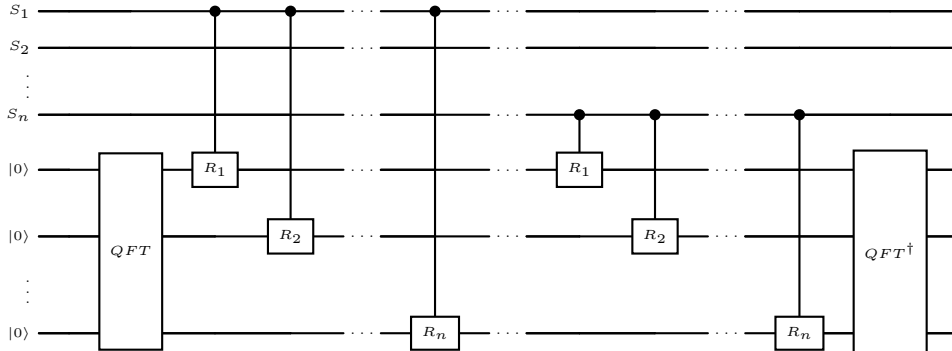


Figure 16: the implementation of QPE using the operator $R_n^{\otimes n}$ for counting the number of charging stations in the state $|S_n \dots S_2 S_1\rangle$. The count will be saved in ancillary qubits. QFT refers to the quantum Fourier transform.

To select the combination with the fewest charging stations, the Hamming weights are compared against a threshold, denoted as τ . For this task, Qiskit's IntegerComparator is employed to evaluate

the weights in relation to τ :

$$|\mathcal{H}(\Phi)\rangle |0\rangle \rightarrow |\mathcal{H}(\Phi)\rangle |\mathcal{H}(\Phi) < \tau\rangle \quad (31)$$

This operator initially requires as many ancillary qubits as input qubits, specifically $\lceil \log(n+1) \rceil$ qubits, but ultimately stores the result of the comparison on a single qubit.

With the methodology established for identifying valid combinations and counting their charging stations, we can mark those with counts below a specified threshold. Combining these insights, Grover's search algorithm can be employed to find valid combinations with charging station counts less than a threshold τ .

Figure ?? illustrates the quantum circuit for a single Grover iteration. The circuit consists of $|\mathcal{Q}|(n+2) + n + \max\{2\lceil \log(n+1) \rceil, n+1\} + 4$ qubits in total. Of these, $n+2$ qubits are allocated to represent the origin, destination, and n corridor nodes. One qubit is initialized in $|-\rangle$ and is used for phase flipping. The remaining qubits serve as ancillary qubits, which are restored at the end of each iteration. The subroutine *Valid* is the oracle described in Section 5.1, Figure 15. It identifies and marks valid combinations that can support all the trips. After marking, the \mathcal{H} subroutine counts the number of charging stations within each combination and encodes the result onto the ancillary qubits. The comparator then compares these counts to a predefined threshold, τ , and marks combinations with fewer charging stations than τ . A controlled-controlled-not (CCNOT) gate flips the phase of combinations that are both valid and contain fewer than τ charging stations. The next three subroutines (*Valid*[†], \mathcal{H} [†] and *compare*[†]) undo the previous operations, and restore the qubits for subsequent Grover iterations. Finally, the diffuser operator amplifies the probability of measuring the solution states by rotating them around the mean.

The action of Grover's diffuser, $2|+^n\rangle\langle +^n| - I$, on the arbitrary state $|\psi_3\rangle$ is:

$$(2|+^n\rangle\langle +^n| - I)|\psi_3\rangle = 2|+^n\rangle\langle +^n|\psi_3\rangle - |\psi_3\rangle = \begin{cases} |\psi_3\rangle & \text{if } |\psi_3\rangle = |+^n\rangle \\ -|\psi_3\rangle & \text{otherwise} \end{cases} \quad (32)$$

Figure 18 illustrates the circuit that flips the phase of a state when it is $|+^n\rangle$ and leaves it unchanged otherwise. This operation contrasts with the description in Equation (32); however, in quantum

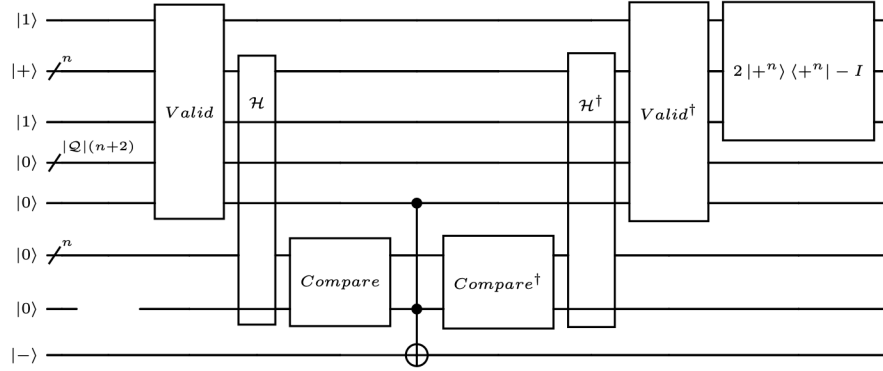


Figure 17: Quantum circuit for one iteration of Grover's Subroutine in optimal charging station placement: Marks valid round-trip combinations, counts and filters those below a threshold, resets ancillary qubits, and enhances their probability with Grover's diffuser.

computing, the relative phase of qubits is crucial while the global phase can be disregarded. Hence, by distinguishing $|+^n\rangle$ from other states through phase flipping, this circuit functions equivalently to the diffuser transformation.

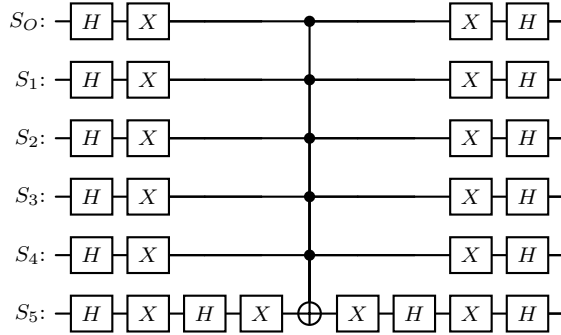


Figure 18: Grover's Diffuser

By iteratively updating τ , the circuit shown in Figure 17 serves as a subroutine to identify the combination with the minimum number of charging stations that supports a round trip. Algorithm 3 outlines the procedure for finding the optimal solution, combining the insights from Algorithms 1 and 2. In this process, the circuit in Figure 17 replaces the black-box functions f and T .

Algorithm 3 Procedure for Determining Ideal Locations for Charging Stations

```
1: run_time, m, best_result,  $\lambda \leftarrow 0, 1, \text{None}, 1.34$ 
2: Choose an integer  $\tau$  uniformly at random such that:  $0 \leq \tau < |\mathcal{N}|$ 
3: while  $\text{run\_time} \leq 22.5\sqrt{2^{|\mathcal{N}|}} + 1.4|\mathcal{N}|$  do
4:   Create a quantum circuit with  $|\mathcal{Q}||\mathcal{N}| + 2|\mathcal{Q}| + |\mathcal{N}| + \max\{2\lceil\log(|\mathcal{N}| + 1)\rceil, |\mathcal{N}| + 1\} + 4$  qubits
5:   Initialize the first  $|\mathcal{N}| + 2$  qubits to  $|1\rangle|+\rangle^{\otimes|\mathcal{N}|}|1\rangle$ , and the last qubit to  $|-\rangle$ 
6:   Choose an integer  $j$  uniformly at random such that:  $0 \leq j < m$ 
7:    $\text{run\_time} += |\mathcal{N}| + j$ 
8:   Apply  $j$  iterations of the subroutine in figure 17
9:   Measure the  $|\mathcal{N}|$  qubits corresponding to the network nodes, and save it in  $i$ 
10:  if  $\text{Valid}(i) = 1$  &  $\mathcal{H}(i) < \tau$  then
11:     $\tau \leftarrow \mathcal{H}(i)$ 
12:     $m \leftarrow 1$ 
13:     $\text{best\_result} \leftarrow i$ 
14:  else
15:     $m \leftarrow \min(\lambda m, \sqrt{2^{|\mathcal{N}|}})$ 
16:  end if
17: end while
18: return  $\text{best\_result}$ 
```

6 Analysis and Results

In this section, algorithm 3 is used to determine the optimal charging station locations in the central Illinois network, as illustrated in Figure 19. The goal is to facilitate travel between the most populated cities in central Illinois: Champaign, Bloomington, Decatur, Springfield, Peoria, and Galesburg. Lincoln serves as a hub in this network, though no trips either originate from or are destined for this city. The map in Figure 19 was converted into a network, depicted in Figure 20, where each edge represents the distance between connected nodes in miles. The driving range for this problem is $R = 260$ miles. The main objective is to determine the optimal combination of charging station locations that can accommodate all possible trips while minimizing the total number of stations needed.

Although gate-based quantum computers with over 1000 quantum bits are currently available [60], they remain noisy, and implementing error-correcting codes is beyond the scope of this study. As a result, IBM's AER simulator was employed, but it is limited in the size of circuits it can process. Due to this constraint, the most qubit-intensive part of the algorithm, the construction of the Valid subroutine, was implemented using the `PhaseOracle` object from IBM's Qiskit framework.

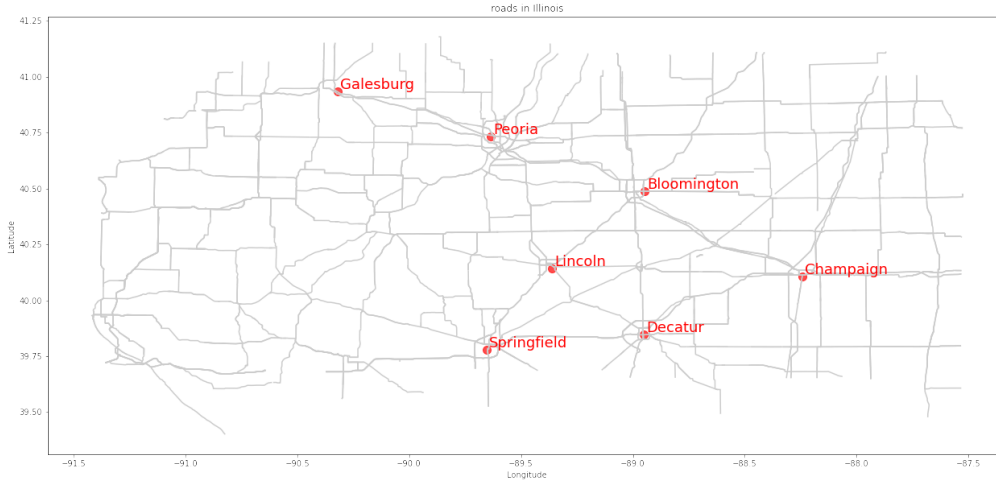


Figure 19: Map of Central Illinois Highlighting Major Roads and Key Cities.

Qiskit is an open-source SDK designed for working with IBM’s quantum computers. The `PhaseOracle` object utilizes a synthesis method that combines the Pseudo-Kronecker Reed-Muller (PKRM) [61] and exclusive-or sum-of-products phase (ESOP-Phase) [62] approaches to convert logical expressions into optimized quantum circuits. The input to the `PhaseOracle` is a logical expression, and the output is a quantum circuit that flips the phase of the quantum states for which the logical expression evaluates to true. This process involves first transforming the logical expression into its Positive Polarity Reed-Muller (PPRM) representation. Then, the Phase-ESOP technique is applied to each Reed-Muller function, converting it into an equivalent quantum circuit. Finally, the gates corresponding to each Reed-Muller function are combined using the pseudo-Kronecker representation to construct the overall quantum circuit.

Equation (33) is the logical expression for the problem constraints, given in equations (2) to (4), which is used as the input to the `PhaseOracle`. A helpful clarification is that the output circuit from the `PhaseOracle` is designed to flip the phase of the states. However, in this case, we require a circuit that marks valid states by flipping $|v_T\rangle$ from $|0\rangle$ to $|1\rangle$. This can be achieved by employing the output circuit as a controlled gate.

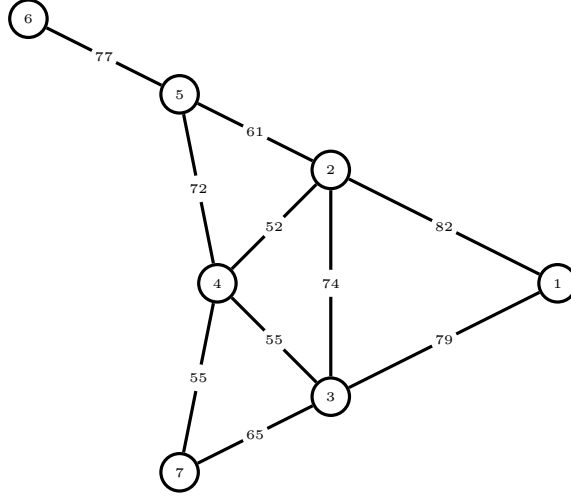


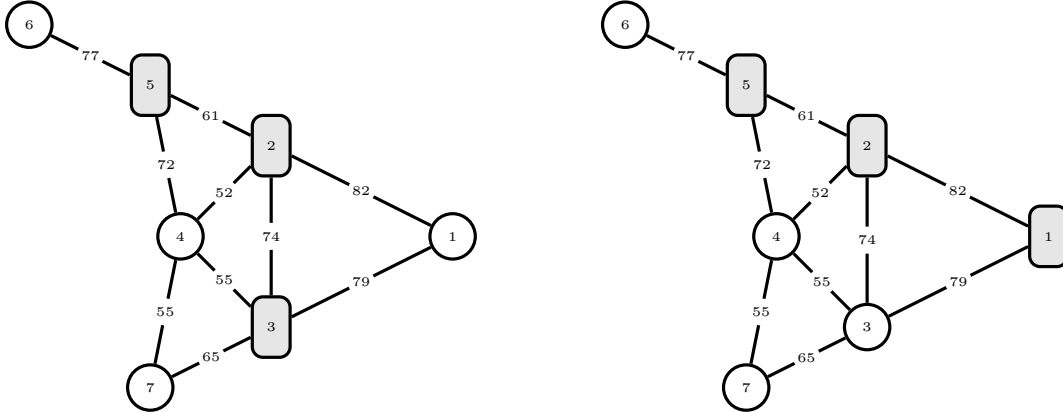
Figure 20: Graph Representation of Central Illinois: Nodes Represent Cities and Edges Denote Distances Between Connected Cities. The nodes correspond to the following cities: 1: Champaign, 2: Bloomington, 3: Decatur, 4: Lincoln, 5: Peoria, 6: Galesburg, 7: Springfield.

$$(S_O \wedge S_D) \wedge \bigcup_{q \in Q} \bigcup_{i \in \mathcal{N}_q} \left(\sim S_i \vee \bigcup_{j \in A_i^q} S_j \right) \quad (33)$$

After constructing the Valid subroutine, the remaining steps follow the same process as described in section 5. Since Algorithm 3 yields the optimal solution with a probability of 0.5, repeating the algorithm 7 times ensures a 0.99 probability of obtaining the optimal solution. Table 4 summarizes the algorithm’s returns. Experiments 2, 3 and 7 yielded the optimal solution, identifying a total of 3 charging stations. In Experiment 4, the algorithm was initialized with a threshold lower than the minimum number of required charging stations, resulting in no feasible solution. The remaining experiments produced suboptimal solutions, each with a total of 4 charging stations. Figure 21 illustrates the optimal configurations of charging stations.

Experiment	1	2	3	4	5	6	7
Initial τ	6	7	6	2	6	4	6
Best Result	0110101	0110100	0110100	None	1010101	1010101	1010100

Table 4: Results of running Algorithm 3 7 times. Experiments 2, 3 and 7 yielded the optimal results.



(a) Nodes 2, 3, and 5 require charging stations.

(b) Nodes 1, 3, and 5 require charging stations.

Figure 21: Optimal charging station locations in the central Illinois network for different sets of nodes requiring charging stations.

7 Conclusion and future path

The installation of public EV chargers along interstate highways is essential for accelerating the transition from gasoline-powered to electric vehicles. However, planning the placement of these charging stations for large networks poses a significant challenge, as it falls under the category of NP-hard problems. Exact methods, such as branch and bound, are computationally demanding. Heuristic and metaheuristic approaches also have limitations in converging to the optimal solution. In response, this study introduces a quantum optimization algorithm that utilizes Grover’s search and quantum phase estimation to identify the optimal combination of charging station locations for long-distance trips. The results indicate that the proposed approach ensures that all vehicles can complete their round trips without encountering battery depletion. The algorithm is resource-efficient, as it reuses ancillary qubits. It also offers a quadratic speedup compared to classical exact methods ($\mathcal{O}(1.4^n)$ versus $\mathcal{O}(2^n)$), thereby enabling a more efficient determination of optimal charging station locations. Future work could extend this method to incorporate additional constraints, such as charging stations with limited capacities or reliability, using the same underlying logic.

References

- [1] Environmental Protection Agency. Inventory of u.s. greenhouse gas emissions and sinks: 1990-2021. <https://www.epa.gov/ghgemissions/inventory-us-greenhouse-gas-emissions-and-sinks-1990-2021>, 2023. EPA 430-R-23-002.
- [2] ON CLIMATE CHANGE et al. Intergovernmental panel on climate change. *World Meteorological Organization*, 52, 2007.
- [3] Francesco Del Pero, Massimo Delogu, and Marco Pierini. Life cycle assessment in the automotive sector: A comparative case study of internal combustion engine (ice) and electric car. *Procedia Structural Integrity*, 12:521–537, 2018.
- [4] R Nealer and TP Hendrickson. Review of recent lifecycle assessments of energy and greenhouse gas emissions for electric vehicles. *Current Sustainable/Renewable Energy Reports*, 2:66–73, 2015.
- [5] Jianping Wen, Dan Zhao, and Chuanwei Zhang. An overview of electricity powered vehicles: Lithium-ion battery energy storage density and energy conversion efficiency. *Renewable Energy*, 162:1629–1648, 2020.
- [6] Hector Campello-Vicente, Ramon Peral-Orts, Nuria Campillo-Davo, and Emilio Velasco-Sanchez. The effect of electric vehicles on urban noise maps. *Applied Acoustics*, 116:59–64, 2017.
- [7] Peter J Fontaine. Shortening the path to energy independence: a policy agenda to commercialize battery–electric vehicles. *The Electricity Journal*, 21(6):22–42, 2008.
- [8] Pedro Nunes, Tiago Farias, and Miguel C Brito. Enabling solar electricity with electric vehicles smart charging. *Energy*, 87:10–20, 2015.
- [9] Asif Khan, Saim Memon, and Tariq Pervez Sattar. Analyzing integrated renewable energy and

- smart-grid systems to improve voltage quality and harmonic distortion losses at electric-vehicle charging stations. *IEEE Access*, 6:26404–26415, 2018.
- [10] Alternative Fuels Data Center. Vehicle registration counts by state. Retrieved June 20, 2024, from <https://afdc.energy.gov/vehicle-registration>. Accessed: 2024-06-20.
- [11] Sanya Carley, Rachel M Krause, Bradley W Lane, and John D Graham. Intent to purchase a plug-in electric vehicle: A survey of early impressions in large us cites. *Transportation Research Part D: Transport and Environment*, 18:39–45, 2013.
- [12] André Hackbarth and Reinhard Madlener. Consumer preferences for alternative fuel vehicles: A discrete choice analysis. *Transportation Research Part D: Transport and Environment*, 25:5–17, 2013.
- [13] Alexandros Dimitropoulos, Piet Rietveld, and Jos N Van Ommeren. Consumer valuation of changes in driving range: A meta-analysis. *Transportation Research Part A: Policy and Practice*, 55:27–45, 2013.
- [14] Viktoria Gass, Johannes Schmidt, and Erwin Schmid. Analysis of alternative policy instruments to promote electric vehicles in austria. *Renewable Energy*, 61:96–101, 2014.
- [15] Martino Tran, David Banister, Justin DK Bishop, and Malcolm D McCulloch. Simulating early adoption of alternative fuel vehicles for sustainability. *Technological Forecasting and Social Change*, 80(5):865–875, 2013.
- [16] John Krumm. How people use their vehicles: Statistics from the 2009 national household travel survey. Technical report, SAE Technical Paper, 2012.
- [17] U.S. Department of Energy and U.S. Environmental Protection Agency. Fueleconomy.gov. <https://www.fueleconomy.gov>. Accessed November 7, 2023.
- [18] Ella Graham-Rowe, Benjamin Gardner, Charles Abraham, Stephen Skippon, Helga Dittmar, Rebecca Hutchins, and Jenny Stannard. Mainstream consumers driving plug-in battery-electric

- and plug-in hybrid electric cars: A qualitative analysis of responses and evaluations. *Transportation Research Part A: Policy and Practice*, 46(1):140–153, 2012.
- [19] Patrick Jochem, Carsten Brendel, Melanie Reuter-Oppermann, Wolf Fichtner, and Stefan Nickel. Optimizing the allocation of fast charging infrastructure along the german autobahn. *Journal of Business Economics*, 86:513–535, 2016.
- [20] Mouna Kchaou-Boujelben. Charging station location problem: A comprehensive review on models and solution approaches. *Transportation Research Part C: Emerging Technologies*, 132:103376, 2021.
- [21] Albert YS Lam, Yiu-Wing Leung, and Xiaowen Chu. Electric vehicle charging station placement: Formulation, complexity, and solutions. *IEEE Transactions on Smart Grid*, 5(6):2846–2856, 2014.
- [22] Zhaoyao Bao and Chi Xie. Optimal station locations for en-route charging of electric vehicles in congested intercity networks: A new problem formulation and exact and approximate partitioning algorithms. *Transportation Research Part C: Emerging Technologies*, 133:103447, 2021.
- [23] Christoph Durr and Peter Hoyer. A quantum algorithm for finding the minimum. *arXiv preprint quant-ph/9607014*, 1996.
- [24] A Yu Kitaev. Quantum measurements and the abelian stabilizer problem. *arXiv preprint quant-ph/9511026*, 1995.
- [25] M John Hodgson. A flow-capturing location-allocation model. *Geographical analysis*, 22(3):270–279, 1990.
- [26] Michael Kuby and Seow Lim. The flow-refueling location problem for alternative-fuel vehicles. *Socio-Economic Planning Sciences*, 39(2):125–145, 2005.
- [27] Ismail Capar and Michael Kuby. An efficient formulation of the flow refueling location model for alternative-fuel stations. *Iie Transactions*, 44(8):622–636, 2012.

- [28] Seyyed A MirHassani and Roozbeh Ebrazi. A flexible reformulation of the refueling station location problem. *Transportation Science*, 47(4):617–628, 2013.
- [29] Mehrnaz Ghamami, Ali Zockaie, and Yu Marco Nie. A general corridor model for designing plug-in electric vehicle charging infrastructure to support intercity travel. *Transportation Research Part C: Emerging Technologies*, 68:389–402, 2016.
- [30] Paul Benioff. The computer as a physical system: A microscopic quantum mechanical hamiltonian model of computers as represented by turing machines. *Journal of statistical physics*, 22:563–591, 1980.
- [31] A Morvan, B Villalonga, X Mi, S Mandra, A Bengtsson, PV Klimov, Z Chen, S Hong, C Erickson, IK Drozdov, et al. Phase transition in random circuit sampling. *arXiv preprint arXiv:2304.11119*, 2023.
- [32] Frank Arute, Kunal Arya, Ryan Babbush, Dave Bacon, Joseph C Bardin, Rami Barends, Rupak Biswas, Sergio Boixo, Fernando GSL Brandao, David A Buell, et al. Quantum supremacy using a programmable superconducting processor. *Nature*, 574(7779):505–510, 2019.
- [33] Google AI Quantum, Collaborators*†, Frank Arute, Kunal Arya, Ryan Babbush, Dave Bacon, Joseph C Bardin, Rami Barends, Sergio Boixo, Michael Broughton, Bob B Buckley, et al. Hartree-fock on a superconducting qubit quantum computer. *Science*, 369(6507):1084–1089, 2020.
- [34] Brian Swingle. Unscrambling the physics of out-of-time-order correlators. *Nature Physics*, 14(10):988–990, 2018.
- [35] David Layden, Guglielmo Mazzola, Ryan V Mishmash, Mario Motta, Pawel Wocjan, Jin-Sung Kim, and Sarah Sheldon. Quantum-enhanced markov chain monte carlo. *Nature*, 619(7969):282–287, 2023.
- [36] Lov K Grover. A fast quantum mechanical algorithm for database search. In *Proceedings of the twenty-eighth annual ACM symposium on Theory of computing*, pages 212–219, 1996.

- [37] Daniel R Simon. On the power of quantum computation. *SIAM journal on computing*, 26(5):1474–1483, 1997.
- [38] Peter W Shor. Polynomial-time algorithms for prime factorization and discrete logarithms on a quantum computer. *SIAM review*, 41(2):303–332, 1999.
- [39] Frédéric Magniez, Ashwin Nayak, Jérémie Roland, and Miklos Santha. Search via quantum walk. In *Proceedings of the thirty-ninth annual ACM symposium on Theory of computing*, pages 575–584, 2007.
- [40] Aram W Harrow, Avinatan Hassidim, and Seth Lloyd. Quantum algorithm for linear systems of equations. *Physical review letters*, 103(15):150502, 2009.
- [41] Tadashi Kadowaki and Hidetoshi Nishimori. Quantum annealing in the transverse ising model. *Physical Review E*, 58(5):5355, 1998.
- [42] Roman Martoňák, Giuseppe E Santoro, and Erio Tosatti. Quantum annealing of the traveling-salesman problem. *Physical Review E—Statistical, Nonlinear, and Soft Matter Physics*, 70(5):057701, 2004.
- [43] Davide Venturelli, D Marchand, and Galo Rojo. Job shop scheduling solver based on quantum annealing. In *Proc. of ICAPS-16 Workshop on Constraint Satisfaction Techniques for Planning and Scheduling (COPLAS)*, pages 25–34, 2016.
- [44] Edward Farhi, Jeffrey Goldstone, and Sam Gutmann. A quantum approximate optimization algorithm. *arXiv preprint arXiv:1411.4028*, 2014.
- [45] Minh Do, Zhihui Wang, Bryan O’Gorman, Davide Venturelli, Eleanor Rieffel, and Jeremy Frank. Planning for compilation of a quantum algorithm for graph coloring. In *ECAI 2020*, pages 2338–2345. IOS Press, 2020.
- [46] Alberto Peruzzo, Jarrod McClean, Peter Shadbolt, Man-Hong Yung, Xiao-Qi Zhou, Peter J Love, Alán Aspuru-Guzik, and Jeremy L O’Brien. A variational eigenvalue solver on a photonic quantum processor. *Nature communications*, 5(1):4213, 2014.

- [47] Abhinav Kandala, Antonio Mezzacapo, Kristan Temme, Maika Takita, Markus Brink, Jerry M Chow, and Jay M Gambetta. Hardware-efficient variational quantum eigensolver for small molecules and quantum magnets. *nature*, 549(7671):242–246, 2017.
- [48] Bela Bauer, Dave Wecker, Andrew J Millis, Matthew B Hastings, and Matthias Troyer. Hybrid quantum-classical approach to correlated materials. *Physical Review X*, 6(3):031045, 2016.
- [49] William P Baritompa, David W Bulger, and Graham R Wood. Grover’s quantum algorithm applied to global optimization. *SIAM Journal on Optimization*, 15(4):1170–1184, 2005.
- [50] Austin Gilliam, Stefan Woerner, and Constantin Gonciulea. Grover adaptive search for constrained polynomial binary optimization. *Quantum*, 5:428, 2021.
- [51] Ashley Montanaro. Quantum speedup of branch-and-bound algorithms. *Physical Review Research*, 2(1):013056, 2020.
- [52] Ashley Montanaro. Quantum walk speedup of backtracking algorithms. *arXiv preprint arXiv:1509.02374*, 2015.
- [53] Mauro Faccin, Tomi Johnson, Jacob Biamonte, Sabre Kais, and Piotr Migdał. Degree distribution in quantum walks on complex networks. *Physical Review X*, 3(4):041007, 2013.
- [54] Andrew M Childs and Jeffrey Goldstone. Spatial search by quantum walk. *Physical Review A—Atomic, Molecular, and Optical Physics*, 70(2):022314, 2004.
- [55] Poojith U Rao and Balwinder Sodhi. Hybrid quantum-classical solution for electric vehicle charger placement problem. *Soft Computing*, 27(18):13347–13363, 2023.
- [56] Mayowa Ayodele. Penalty weights in qubo formulations: Permutation problems. In *European Conference on Evolutionary Computation in Combinatorial Optimization (Part of EvoStar)*, pages 159–174. Springer, 2022.
- [57] Aman Chandra, Jitesh Lalwani, and Babita Jajodia. Towards an optimal hybrid algorithm for ev charging stations placement using quantum annealing and genetic algorithms. In *2022 Inter-*

- national Conference on Trends in Quantum Computing and Emerging Business Technologies (TQCEBT)*, pages 1–6. IEEE, 2022.
- [58] Dandan Hu, Xiongfai Li, Chen Liu, and Zhi-Wei Liu. Integrating environmental and economic considerations in charging station planning: An improved quantum genetic algorithm. *Sustainability*, 16(3):1158, 2024.
- [59] Michel Boyer, Gilles Brassard, Peter Høyer, and Alain Tapp. Tight bounds on quantum searching. *Fortschritte der Physik: Progress of Physics*, 46(4-5):493–505, 1998.
- [60] Jay Gambetta. Ibm quantum computing blog — the hardware and software for the era of quantum utility is here, 2024. Accessed: 2024-10-18.
- [61] DH Green. Hybrid forms of reed-muller expansions. *International journal of electronics*, 81(1):15–35, 1996.
- [62] Giulia Meuli, Bruno Schmitt, Rüdiger Ehlers, Heinz Rienecker, and Giovanni De Micheli. Evaluating esop optimization methods in quantum compilation flows. In *Reversible Computation: 11th International Conference, RC 2019, Lausanne, Switzerland, June 24–25, 2019, Proceedings 11*, pages 191–206. Springer, 2019.